Molecular Crystals and Liquid Crystals

Publication details, including instructions for authors and subscription information:
http://www.tandfonline.com/loi/gmcl20

DISPERSION CURVES COMPUTED FROM CHANNELED DIFFRACTION SPECTRA OF LIQUID CRYSTALS

M. Socaciu [a] & M. Ursache [a]

[a] Department of Physics, University of Craiova, 13 A. I. Cuza, Craiova, 1100, Romania

Version of record first published: 02 Feb 2011

To cite this article: M. Socaciu & M. Ursache (2003): DISPERSION CURVES COMPUTED FROM CHANNELED DIFFRACTION SPECTRA OF LIQUID CRYSTALS, Molecular Crystals and Liquid Crystals, 403:1, 1-13

To link to this article: http://dx.doi.org/10.1080/744818941

Mol. Cryst. Liq. Cryst., Vol. 403, pp. 1–13, 2003

ISSN: 1542-1406 print/1563-5287 online
DOI: 10.1080/15421400390233968

Taylor & Francis
Taylor & Francis Group

DISPERSION CURVES COMPUTED FROM CHANNELED DIFFRACTION SPECTRA OF LIQUID CRYSTALS

M. Socaciu and M. Ursache*
Department of Physics, University of Craiova, 13 A. I. Cuza, Craiova, 1100, Romania

Using a new version of the Talbot-Rayleigh method we recorded the I (λ) channeled spectra of uniaxial nematic liquid crystal at different temperatures. We derive the theoretical expression of I (λ) that involves a three-band model for the refractive indices, which is then fitted with the experimental data by a nonlinear optimization procedure. As a result, we compute the dispersion curves n^o, n^e, Δn, their temperature dependencies, and the band contributions.

Keywords: Dispersion curves, channeled diffraction spectra

INTRODUCTION

In this article we propose a method which gives a rigorous theoretical interpretation of the channeled spectra produced by an interferometry setup with diffraction grating inserted in order to compute the dispersion curves and band contributions, having the temperature as an external parameter, for an uniaxial medium.

We choose the liquid crystal only as an example, in order to easily compare our results with the corresponding ones previously reported. However, our method can be applied to any transparent anisotropic material, being not restricted to liquid crystals. From channeled diffraction spectra we obtained quasi-continuum spectra for the indices dispersion, having obvious advantages, especially for new synthesized liquid crystals.

Until now many studies have been devoted to refractive indices measurements of liquid crystals using an Abbe refractometer, thin prism

Received 21 March 2000; accepted 5 June 2003.
*Corresponding author. E-mail: msocaciu@central.ucr.ro

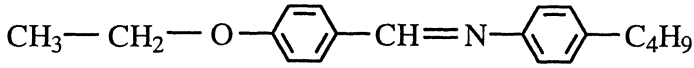

FIGURE 1 Molecular structure of nematic liquid crystal EBBA.

technique [1], and the wedge method [2,3], which provide $n^{\circ}(T)$, $n^{e}(T)$, a Jelly-Leitz refractometer [4] giving discrete dispersion spectra, Fabry-Perot interference method [5], and Rayleigh-Talbot method [6,7] measuring quasicontinuum spectra. Much work has been done to investigate the physical origins of the birefringence [8–10] which depends on the packing density of liquid crystal molecules, the available electrons per molecule, the degree of order, the wavelength, and by the resonance anisotropy of electronic transitions.

In this article we also present the experimental method for recording the channeled spectra $I(\lambda)$ of (p-etoxybenzylidene-)-p-n-butylaniline (EBBA) nematic liquid crystal with the molecular structure given in Figure 1.

The spectra were recorded with parallel polarizer and analyzer orientated along parallel and normal directions with respect to the optical axis in the sample, at different temperatures.

Afterwards we derive the theoretical expression of $I(\lambda)$, assuming a three-band model for the ordinary and extraordinary indices. Consequently, we determine the refractive indices as well as the birefringence dispersion at different temperatures. We also study the absorption bands contributions to these dispersion curves.

By using a nonlinear fitting procedure, we deduce all the parameters involved in the calculation of $n^{o}(\lambda)$, $n^{e}(\lambda)$. We are thus able to determine the refractive indices and birefringence dispersion, the band contributions to these curves, and their temperature dependencies.

Moreover, our method, which will be described in this article, proves to be a fast and high precision one which eliminates the necessity of the so-called "reference point" measurements or a previous recording of the polarized absorption spectra and the uncertainty of the usual method in the correlation between the x coordinate in the output plane and the wavelength values.

EXPERIMENTAL MEASUREMENTS

The nematic aligned mesophase of calamitic liquid crystals constitute a standard example for uniaxial medium. Their rodlike molecules have the long axis line up parallel to a preferred direction represented by the vector director and exhibit a free rotation around the director. A uniaxial nematic

liquid crystal is an optically anisotropic medium, and its optical anisotropy is large and controllable by the temperature and by the external field.

The experimental channeled spectra was recorded using a white light source and a lens that provides a parallel beam. This beam is then split in two components, one of them passing through the reference material while the second one passes through the liquid crystal sample, which may be treated as a transparent plane-parallel plate placed normal to the light propagation direction. Both beams are incident on a diffraction grating with $p = 175 \cdot 10^{-6}$ m grating constant. The diffracted beams are focused on the image plane by a second lens. The interference channeled spectrum obtained in the first order diffraction maximum is recorded by a CCD linear array connected to a computer via DAS 1601 interface operating in direct memory access mode for a fast acquisition process.

In order to calibrate the sensor in terms of wavelength values, a set of interference filters was used such that the x coordinate of the diffraction maxima was determined and we were able to draw the resulting $x(\lambda)$ curve. The exposure time is modified by a pulse generator which gives the triggering signal for data acquisition simultaneously. A monitoring oscilloscope for a direct investigation of the channeled spectrum shapes has been also used.

In Figure 2 we present the sandwich-type cell which was half filled by capillarity with a uniaxial nematic liquid crystal (5), (p-etoxy-benzylidene)-p-n-butylaniline (EBBA). In the second half of the cell we inserted a 180 μm thick glass plate (3) as distancer and as a reference material which assures a uniform thickness of the cell. The sample was placed such that

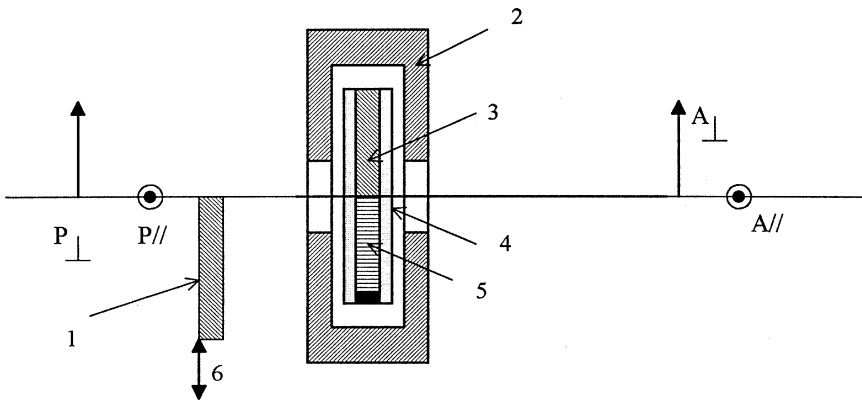

FIGURE 2 Sample geometry to study the channeled spectra: 1,4 compensatory plate; 2 special electric oven; 3, reference material; 4, optical glass plates of the cell; 5 nematic liquid crystal; 6 (x − y) displacement mechanism.

the separation line between the reference material and the liquid crystal is along the symmetry axis of the experimental setup. In order to eliminate the optical path modification induced by the distancer glass plate, a compensatory plate (1) made from the same glass and having the same thickness was interposed in front of the liquid crystal using an $x-y$ displacement mechanism (6).

For the determination of the liquid crystal birefringence the sample must be a monocrystal with a well known molecular alignment and optical axis direction. The glass plates (4) of the liquid crystal cell were well rubbed to insure a homogeneous planar texture of the nematic monocrystal which is verified by using a polarized light microscope with crossed polarizers.

In the case of liquid crystals, the easiest way to obtain the extraordinary index is to have a homogeneous planar texture between two polarizers parallel to the optical axis of the nematic liquid crystal cell. After a quarter turn of both polarizers the ordinary index is obtained.

The cell is placed within a special electric oven (2) which is connected to a temperature controller such that the sample was cooled and heated with 1°C/min linear temperature rate. The temperature was measured with a constantan-copper thermocouple connected to a KEITHLEY 2000 multimeter with 0.01°C precision.

In conclusion, the only measurements we had to perform were the $I(\lambda)$ spectra at different temperature values, for parallel and normal orientations of both parallel polarizers with respect to the optical axis in the cell. An example of such a channeled spectrum is given in Figure 3 for the temperature $T = 50$°C and parallel orientation of the polarizers.

THEORY

Theoretical Channeled Spectra

The first step of our method consists of establishing the theoretical expression of the intensity $I(\lambda)$, starting with the amplitude of an arbitrary wave emerging from a point that has an x coordinate under the diffraction angle θ:

$$da = T(x)\exp(i\varphi(x))dx \tag{1}$$

where

$$T(x) = \begin{cases} T_1, & x \in (-\infty, 0) \\ 1, & x \in (0, \infty) \end{cases} \tag{2}$$

and T_1 is the transmission coefficient of the liquid crystal half-cell. Most of liquid crystal materials have their absorption bands in IR and/or UV spectral region, so that in the visible domain we can assume that the transmission

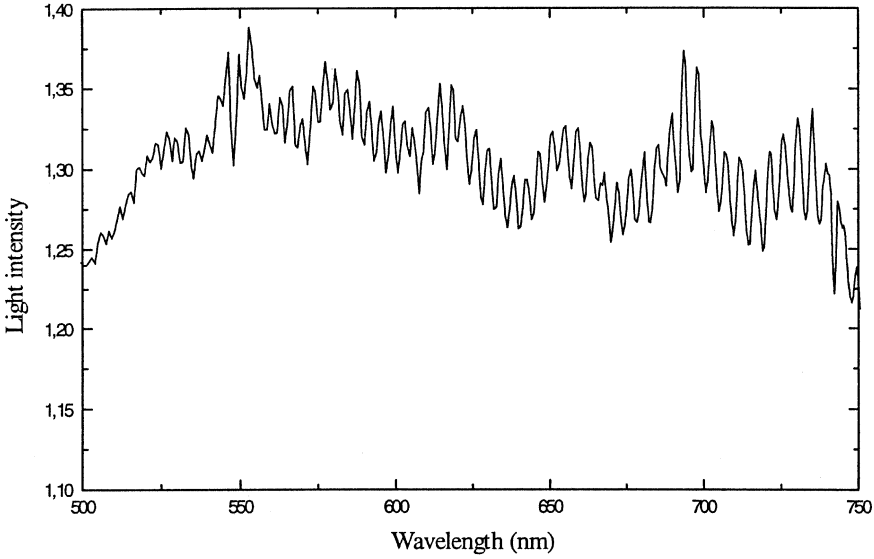

FIGURE 3 The experimental channeled spectrum $I(\lambda)$ at $T = 50°C$.

coefficient is practically constant. The upper and lower limits in the expression of $T(x)$ are considered to be infinite because the beam is well collimated.

The light phase after the cell and grating is given by:

$$\varphi(x) = \begin{cases} \frac{2\pi}{\lambda}[x\theta + (n-1)d], x \in (-\infty, 0) \\ \frac{2\pi}{\lambda} x\theta, x \in (0, \infty) \end{cases} \tag{3}$$

The amplitude of the resulting wave in an arbitrary point of the image-plane is then:

$$\begin{aligned} a &= \int_{-\infty}^{\infty} da \\ &= \int_{-\infty}^{0} T_1 \exp i\left[\frac{2\pi}{\lambda}(x\theta + (n-1)d)\right] dx + \int_{0}^{\infty} \exp i\left[\frac{2\pi}{\lambda} x\theta\right] dx \end{aligned} \tag{4}$$

where the two terms are the contributions of the sample region and of the free space one, respectively.

Calculating the light intensity in the arbitrary point, making use of the grating periodicity in Equation (4), we obtained:

$$I = \frac{N^2 p^2}{4}\left(\frac{\sin\beta/2}{\beta/2}\right)^2 [A + \cos(\alpha + \beta)] \tag{5}$$

where

$$A = \frac{1 + T_1^2}{2T_1}, \quad \alpha = \frac{2\pi}{\lambda}(n-1)d, \quad \beta = \frac{2\pi}{\lambda}p\theta \tag{6}$$

with p-being the diffraction grating constant and $\sin\theta \approx \theta = x/f, f$ being the focal length of the lens.

The second step of our method consists of choosing the model for the ordinary and extraordinary indices dependence on the wavelength values.

We used the realistic three-band model [9] which accounts for all electronic transitions from the electronic transition spectrum. There are three bands consisting of one λ_0-band ($\sigma - \sigma^*$ transition), and λ_1- and λ_2-bands (two $\pi - \pi^*$ transitions). The liquid crystal molecules usually have delocalized π-electronic structure which makes them potential sources of fast and large optical nonlinearities.

The energy difference between the energy levels σ, π with their excited counterparts σ^*, π^* gives rise to the absorption bands of the molecules, centered on $\lambda_0, \lambda_1, \lambda_2$.

The model is described, for $\lambda \gg \lambda_0$ in the off-resonance region by the expression

$$n^{e,o}(\lambda) \cong 1 + n_0^{e,o} + g_1^{e,o}\frac{\lambda^2\lambda_1^2}{\lambda^2 - \lambda_1^2} + g_2^{e,o}\frac{\lambda^2\lambda_2^2}{\lambda^2 - \lambda_2^2} \tag{7}$$

where $n_0^{e,o} = g_0^{e,o}\lambda_0^2$.

The values of $g_i^{e,o}(i = 1, 2)$ determine the external parameter effect on the refractive indices, i.e., the temperature, in our experiment.

The $n^{e,o}(\lambda)$ dependence given in Equation (7) was inserted into the α formula in Equation (6), which in turn has been replaced in Equation (5) such that the complete theoretical expression of $I(\lambda)$ is determined.

Band Contributions to Refractive Indices and Birefringence

From the three-band model the contribution of each band to the refractive indices and birefringence can be calculated quantitatively and they depend on the structure and constituents of the liquid crystal.

We derive, in the next step of our method, each band contribution ($C^j_{\lambda_i}(\%)$, where $i = 0$, 1, 2 and $j = n^o, n^e, \Delta n$) to the refractive indices and birefringence. In this respect, we used the following formula for the three-band model:

1. λ_0-band contribution to both refractive indices:

$$C^j_{\lambda_0}(\%) = \frac{n_0^{e,o}}{n_0^{e,o} + g_1^{e,o}\frac{\lambda^2\lambda_1^2}{\lambda^2-\lambda_1^2} + g_2^{e,o}\frac{\lambda^2\lambda_2^2}{\lambda^2-\lambda_2^2}} \tag{8}$$

for $j = n^e, n^o$.

2. λ_0-band contribution to birefringence:

$$C^{\Delta n}_{\lambda_0}(\%) = \frac{n_0^e - n_0^o}{n^e - n^o} \tag{9}$$

3. λ_i-band contribution (i = 1, 2) to both refractive indices:

$$C^j_{\lambda_i}(\%) = \frac{g_i^{e,o}\frac{\lambda^2\lambda_i^2}{\lambda^2-\lambda_i^2}}{n_0^{e,o} + g_1^{e,o}\frac{\lambda^2\lambda_1^2}{\lambda^2-\lambda_1^2} + g_2^{e,o}\frac{\lambda^2\lambda_2^2}{\lambda^2-\lambda_2^2}} \tag{10}$$

for $j = n^e, n^o$.

4. λ_i-band contributions to birefringence:

$$C^{\Delta n}_{\lambda_i}(\%) = \frac{g_i^e\frac{\lambda^2\lambda_i^2}{\lambda^2-\lambda_i^2} - g_i^o\frac{\lambda^2\lambda_i^2}{\lambda^2-\lambda_i^2}}{\Delta n_0 + G_1\frac{\lambda^2\lambda_1^2}{\lambda^2-\lambda_1^2} + G_2\frac{\lambda^2\lambda_2^2}{\lambda^2-\lambda_2^2}} \tag{11}$$

where $G_i = g_i^e - g_i^o, (i = 1, 2)$.

One can see that all the band contributions can be evaluated only if all parameters g_i^e, g_i^o in the formula in Equation (7) are computed.

RESULTS AND DISCUSSION

We used a nonlinear fitting procedure of the Levenberg-Marquardt type in order to determine the values of the unknown parameters $g_i^{e,o}, \lambda_i$, where $i = 0, 1, 2$, in the theoretical expression of $I(\lambda)$ by solving the optimization problem defined by the condition that the "distance" (L^2-norm) between the experimental and theoretical data is minimum. Consequently we concluded that if the number of experimental points increases in a narrow wavelength domain then the agreement between the theoretical and experimental $I(\lambda)$ is better.

We performed the nonlinear fitting of each pair form a large set of experimental and theoretical $I(\lambda)$ curves in order to obtain all the parameters necessary in the formula in Equation (7) for the ordinary and

TABLE 1 Dispersion Curves Parameters

Parameters	50°C	65°C	74°C
n_0^e	0.511110	0.508917	0.506435
n_0^o	0.400343	0.400325	0.400607
g_1^e	2.36206	2.34440	2.33256
g_1^o	1.36183	1.36412	1.36726
g_2^e	1.42210	1.40464	1.39843
g_2^o	0.47002	0.47045	0.47534

TABLE 2 Refractive Indices and Birefringence Dispersion at Different Temperatures

	65°C			74°C		
λ(nm)	n^o	n^e	Δn	n^o	n^e	Δn
481.30	1.54113	1.84443	0.3033	1.54196	1.83997	0.29801
498.56	1.53700	1.83324	0.29624	1.53783	1.82895	0.29112
516.30	1.53345	1.82363	0.29018	1.53426	1.81948	0.28522
533.60	1.53049	1.81570	0.28521	1.53130	1.81167	0.28037
550.47	1.52801	1.80906	0.28105	1.52881	1.80512	0.27631
566.91	1.52590	1.80343	0.27753	1.52669	1.79956	0.27287
582.91	1.52408	1.79860	0.27452	1.52487	1.79480	0.26993
598.48	1.52250	1.79442	0.27192	1.52329	1.79067	0.26738
613.61	1.52113	1.79077	0.26964	1.52191	1.78707	0.26516
628.31	1.51991	1.78758	0.26767	1.52069	1.78392	0.26323
642.57	1.51884	1.78475	0.26591	1.51962	1.78113	0.26151
656.41	1.51789	1.78224	0.26435	1.51866	1.77865	0.25999
669.81	1.51703	1.78001	0.26298	1.51781	1.77644	0.25863
682.77	1.51627	1.77800	0.26173	1.51704	1.77446	0.25742
695.30	1.51558	1.77620	0.26062	1.51635	1.77268	0.25633
707.39	1.51496	1.77457	0.25961	1.51573	1.77107	0.25534
719.06	1.51440	1.77310	0.25870	1.51516	1.76962	0.25446
730.28	1.51388	1.77177	0.25789	1.51465	1.76830	0.25365
741.08	1.51342	1.77056	0.25714	1.51418	1.76710	0.25292
751.44	1.51300	1.76946	0.25646	1.51376	1.76601	0.25225
761.36	1.51261	1.76845	0.25584	1.51337	1.76502	0.25165

extraordinary indices, at different temperature values. Some of these parameters are presented in Table 1 for only three temperature values.

In Table 2 the computed values of $n^o, n^e, \Delta n$ dispersion curves are given for $T = 65°C$ and $T = 74°C$.

As an example we show these dependencies in Figures 4(a) to 4(c), only for the temperature $T = 50°C$.

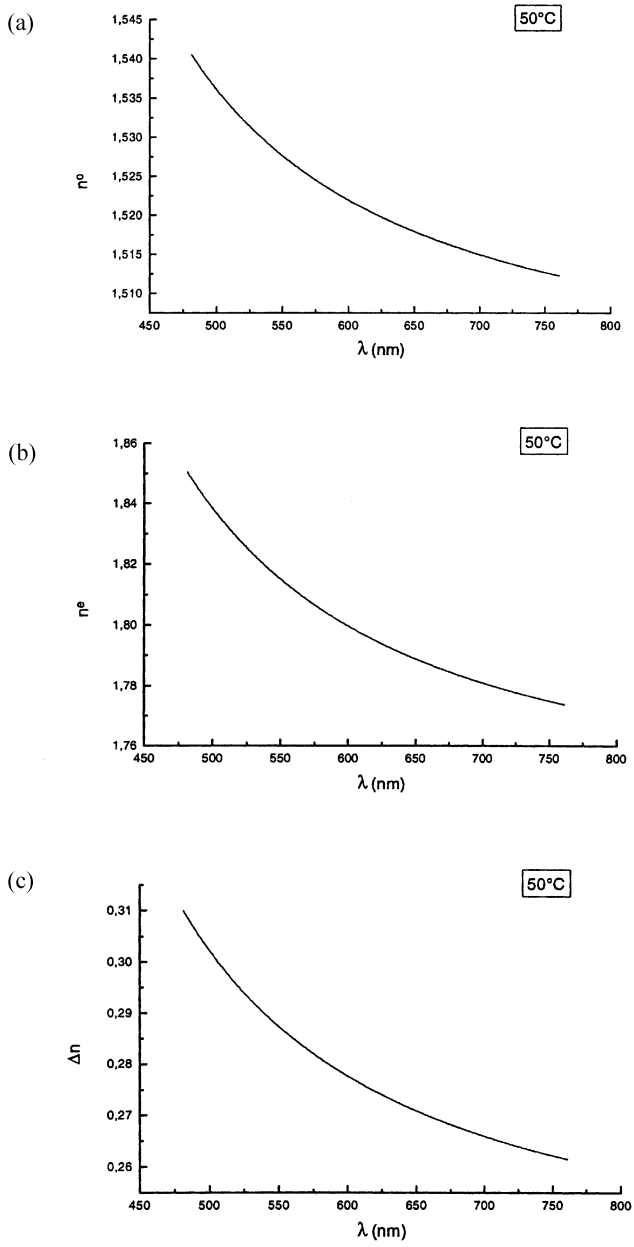

FIGURE 4 The dispersion curves at $T = 50°\mathrm{C}$: (a) $n^o(\lambda)$, (b) $n^e(\lambda)$, (c) $\Delta n(\lambda)$.

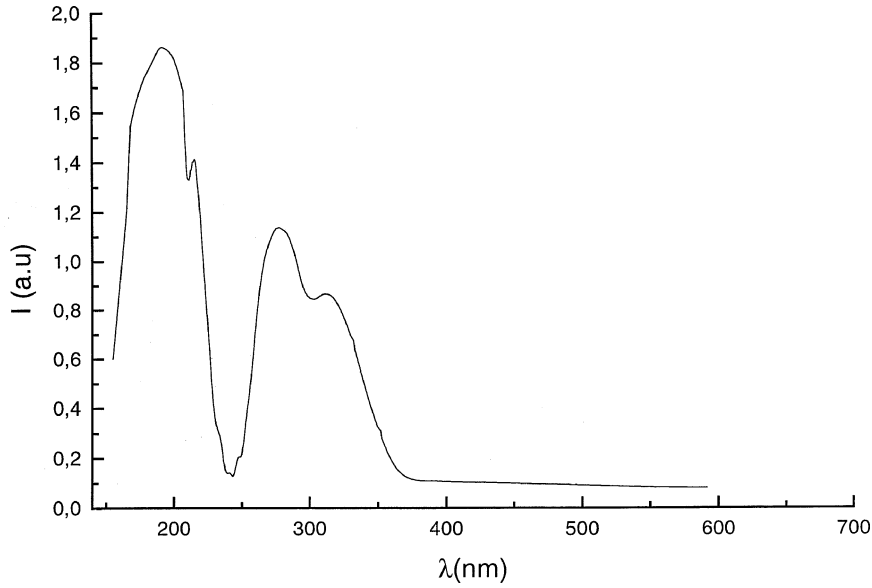

FIGURE 5 The experimental absorbtion UV-visible spectrum of EBBA.

Finally, the $\lambda_0, \lambda_1, \lambda_2$ wavelength values that resulted from our simulations are in the ultraviolet region $\lambda_0 = 123\,\text{nm}$, $\lambda_1 = 203\,\text{nm}$, $\lambda_2 = 304\,\text{nm}$ corresponding to one $\sigma - \sigma^*$ and two $\pi - \pi^*$ electronic transitions. The experimental absorption UV-visible spectrum presented in Figure 5 show that each of our theoretical λ_1, λ_2 values represent exactly the mean wavelength value of the superposition of two neighbor absorption bands.

The experimental absorption spectrum of EBBA was recorded using ethylalcohol as UV spectrophotometric-grade solvent. To avoid saturation problem, we dissolved EBBA in the UV-transparent liquid crystal (LC) the concentration being much smaller than 1 purity and UV transparency required.

In Figures 6(a)to 6(c), we give the graphical representation of the band contributions to $n^o, n^e, \Delta n$ as λ-functions, at $T = 74°\text{C}$ as an example.

It is seen from Figure 6(a) that the λ_0-band contributions to refractive indices is much higher than the contribution to birefringence, in the visible region, due to the high optical density of the $\sigma - \sigma^*$ electronic transitions.

We can also see from Figures 6(b) and 6(c) that the contributions of the $\pi - \pi^*$ electronic transitions (λ_1, λ_2-bands) are dominant in the birefringence and a few times lower in the refractive indices values.

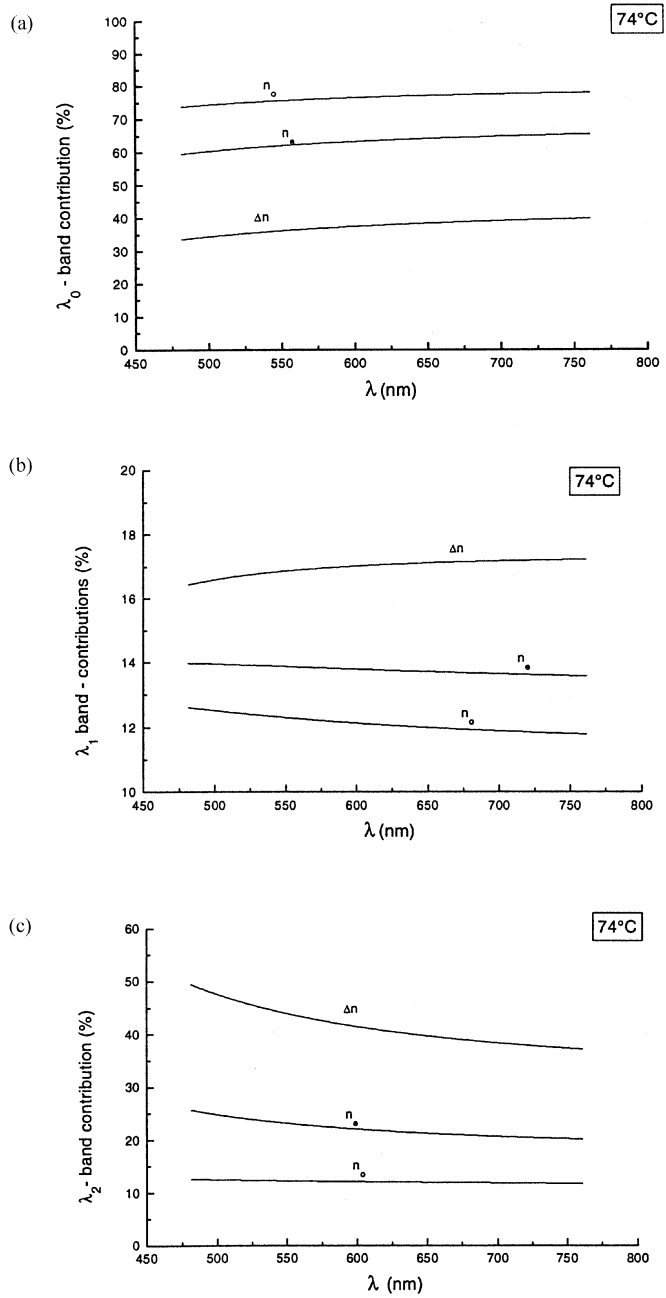

FIGURE 6 Band contributions to $n^o, n^e, \Delta n$ at $T = 74°\text{C}$ (a) λ_0, (b) λ_1, (c) λ_2.

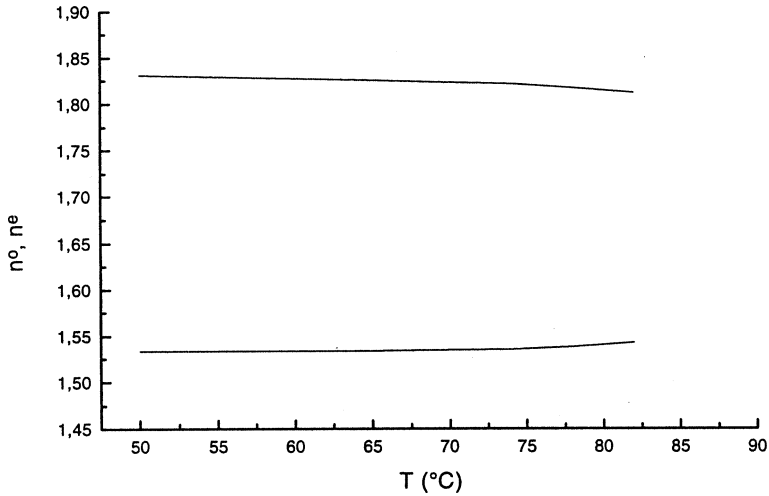

FIGURE 7 Ordinary and extraordinary indices as functions of temperature.

The previous steps of our calculations provide the functions $n^o(\lambda), n^e(\lambda)$ for each temperature value in the measurement domain, allowing us to represent $n^o(T)$ and $n^e(T)$ as in Figure 7 for any wavelength λ.

These values were replaced in the expression of the isotropic electric permittivity:

$$\varepsilon_i = \frac{1}{3}(n^e)^2 + \frac{2}{3}(n^o)^2 \tag{12}$$

and we verified that $\varepsilon_i = 2.67$ for each pair $n^o(T), n^e(T)$ at any temperature.

CONCLUSIONS

In conclusion, the main goal of our study is to describe a fast and high precision procedure to compute both the dispersion curves and the band contributions for uniaxial nematic liquid crystals. The most important advantages of our improved experimental and theoretical method can be summarized as follows.

We eliminated the uncertainty of the usual method in the correlation between the x coordinate in the output plane and the wavelength values by finding a complete polynomial function $x(\lambda)$.

We also avoided the complementary measurements imposed by the previous method which are based on the determination of the channel orders in the $I(\lambda)$ spectra. Our data processing does not require any

$n_{ref}^{o,e}(\lambda, T)$ measurements or a previous recording of the polarized absorption spectra. The accuracy of our method relies as strongly as the known ones on $n_0^{o,e}(T)$ at fixed wavelength, but this time it is a calculated value in good agreement with the experimental results.

All the dispersion curves obtained by our procedure can be extrapolated to the entire spectral domain (from UV to IR), although the measurements are made only in the visible domain, obtaining a very good agreement with the results provided by other methods.

In addition, the accuracy in our quasicontinuum dispersion curves is higher (5.10^{-6}) than the ones reported until now, the data acquisition and processing being efficiently integrated by the proposed technique.

If the measurement domain is well refined in terms of wavelength values then the anomalous dispersion of a liquid crystal which is related to the absorption bands can be identified. By a computer-controlled Fourier-transform spectrometer and using the phase difference measurement technique in both visible and infrared spectral regions [11] the anomalous dispersion domains were noticed.

The same analysis may be easily reproduced for a different external parameter (electric field or temperature and electric field), and the calculations may also be extended to study the order parameter dependence on these factors.

REFERENCES

[1] Mitra, M., Gupta, S., Paul, R., & Paul, S. (1991). *Mol. Cryst. Liq. Cryst.*, *199*, 257.
[2] Hanson, E. G., & Shen, Y. R. (1976). *Mol. Cryst. Liq. Cryst.*, *36*, 193.
[3] Haller, I., Huggins, H. A., & Freiser, M. J. (1972). *Mol. Cryst. Liq. Cryst.*, *16*, 53.
[4] Vaz, N. A., Smith, G. W., Montgomery, G. P., Marion, J. R., & Marion, W. D. (1991). *Mol. Cryst. Liq. Cryst.*, *198*, 305.
[5] Kawaiada, M., Yamaguchi, T., & Akahane, T. (1989). *J. Appl. Phys.*, *28*(9), L1602.
[6] Warrenghem, M., & Joly, G. (1991). *Mol. Liq. Cryst.*, *207*, 205.
[7] Abdulhalim, I. (1991). *Mol. Cryst. Liq. Cryst.*, 197, 103.
[8] Wu, S. T. (1986). *Phys. Rev. A*, *33*(2), 1270.
[9] Wu, S. T. (1991). *J. Appl. Phys.*, *69*(4), 2080.
[10] Boschmans, M. (1991). *Mol. Cryst. Liq. Cryst.*, *199*, 267.
[11] Khoo, I. C., & Wu, S.-T. (1993). *Optics and Nonlinear Optics of Liquid Crystals*, New York: World Scientific.